A comparative physico-chemical study of chlorapatite and hydroxyapatite: from powders to plasma sprayed thin coatings

I Demnati[1], **D Grossin**[1], **C Combes**[1], **M Parco**[2], **I Braceras**[2,3] **and C Rey**[1]

[1] Université de Toulouse, CIRIMAT CNRS-INPT-UPS, ENSIACET, Toulouse, France
[2] Tecnalia, Mikeletegi Pasealekua 2, Teknologi Parkea, E-20009 Donostia-San Sebastian, Spain
[3] Ciber BBN, Mikeletegi Pasealekua 2, 20009 Donostia-San Sebastian, Spain

E-mail: imane.demnati@ensiacet.fr

Abstract

Due to their bioactivity and osteoconductivity, hydroxyapatite (HA) plasma sprayed coatings have been widely developed for orthopedic uses. However, the thermodynamic instability of HA leads frequently to a mixture of phases which limit the functional durability of the coating. This study investigates the plasma spraying of chlorapatite (ClA) powder, known to melt without decomposition, onto pure titanium substrates using a low energy plasma spray system (LEPS). Pure ClA powder was prepared by a solid gas reaction at 950 °C and thermogravimetric analysis showed the good thermal stability of ClA powder in the range 30–1400 °C compared to that of the HA powder. Characterization of ClA coating showed that ClA had a very high crystalline ratio and no other crystalline phase was detected in the coating. HA and ClA coatings composition, microstructure and *in vitro* bioactivity potential were studied, compared and discussed. *In vitro* SBF test on HA and ClA coatings revealed the formation of a poorly crystalline apatite on the coating surface suggesting that we could expect a good osteoconductivity especially for the ClA coating prepared by the LEPS system.

(Some figures may appear in colour only in the online journal)

1. Introduction

Hydroxyapatite (HA) coatings on titanium implants have been developed for orthopedic uses because of their bioactivity and biocompatibility. Thermally sprayed HA coatings on implants have been widely used for over two decades to enhance hard tissue regeneration and attachment (Gross and Berndt 1998, Cheang and Khor 1996, Deram *et al* 2003). The use of a thin coating provides to the implanted devices the bioactive properties of HA complementarily to the load bearing function of the metal.

Because of the coarse minimum particle size technically acceptable for making coatings with the current plasma spray systems, the latter are not precise enough and do not allow the deposition of very thin homogeneous coatings. These difficulties have limited the use of standard plasma spray systems to large implants and, despite early enthusiasm, coated dental implants have not been extensively developed and even have a bad reputation among dentists due to the use of poor quality, irregular and uncontrolled coatings at the beginning of the technical application. Moreover, the HA powder may decompose totally or partially during plasma spraying to give a mixture of crystalline and amorphous phases, especially tricalcium phosphate (TCP) and tetracalcium phosphate (TTCP) and amorphous calcium phosphate (ACP) (Carayon and Lacout 2003, Demnati *et al* 2011). Interestingly, chlorapatite (ClA) however has never been tested in coatings of medical devices despite its ability to melt without decomposition, which could be a decisive advantage (Prener 1971, Tõnsuaadu *et al* 2011).

In a recent study, new low-energy plasma spray systems (LEPS) were designed and applied for the first time in this field

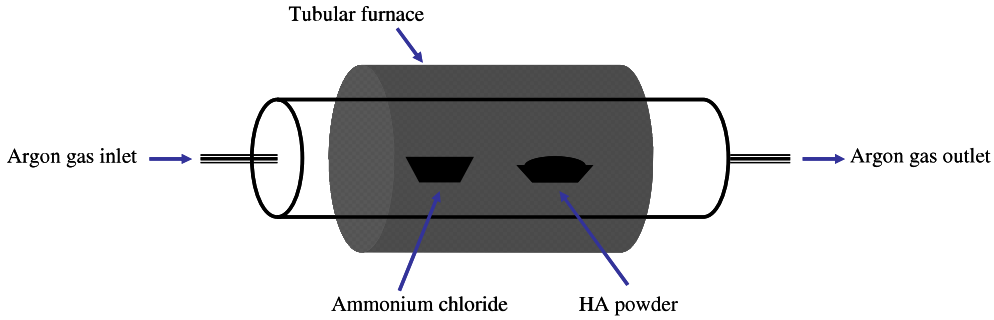

Figure 1. Schema of ClA synthesis experimental setup.

(Demnati *et al* 2011). A more versatile, precise and economical coating process presents progress for companies involved in biomedical coatings, especially in Europe where leadership companies are installed.

Modification of the synthetic HA, for orthopedic and dental applications, by introducing ion substitutes of calcium, phosphate and hydroxide ions have been developed with some success in recent years (Cheng *et al* 2005). The incorporation of species like magnesium, zinc, strontium, fluoride, carbonate and silicate into the apatite structure has been shown to improve the biological response after implantation and/or the stability of the implant/tissue interface. Very few studies have, however, been carried on the substitution of hydroxide by chloride ions, although this element seems to exist as a trace element in the mineral phase of bone and teeth (Elliott 1994, Young and Elliott 1966).

The aim of this work was to compare HA and ClA coatings obtained by a LEPS using the same powders characteristics and spraying parameters in order to minimize the impact of heat and mass transfer difference. Despite their importance in plasma spraying (Pawlowski 2008), these phenomena will not be considered in this work, but we investigated the thermal stability of HA and ClA using thermogravimetric analysis. The coatings obtained were characterized by scanning electron microscopy (SEM) and compositional characterization was investigated using x-ray diffractometry (XRD) and Fourier transform infrared spectroscopy (FTIR). Then the biological properties of the coatings were evaluated using the SBF test proposed by Kokubo (Kokubo 1998).

2. Materials and methods

2.1. Samples preparation

HA powder was provided by Teknimed (l'Union, France). The powder was stoichiometric HA, calcined and granulated to a particle size between 50 and 80 μm. The average particle size was $d_{0.5} = 69.5$ μm. The powder Ca/P atomic ratio was close to stoichiometry (1.67) and the XRD pattern corresponded to pure HA without any other crystalline impurity.

Chlorapatite feedstock powder was prepared through a thermal exchange (gas–solid reaction) at 950 °C during 2 h between the commercial HA powder (Teknimed, France) and sublimated ammonium chloride in a tubular furnace under a dynamic argon atmosphere (figure 1) according to the following reaction:

$$2NH_4Cl + Ca_{10}(PO_4)_6(OH)_2 \rightleftharpoons Ca_{10}(PO_4)_6Cl_2 + 2NH_3 + 2H_2O. \quad (1)$$

The substrate for apatite coatings was a flat medical grade titanium cylinder, which was cut into disc-shaped samples of 12 mm diameter and 3 mm thickness. The Ti discs were blasted, cleaned and degreased. ClA and HA powders were both plasma sprayed onto Ti substrate samples using a novel plasma spray mini-gun operating at low energy (Demnati *et al* 2011). The deposition was performed in air with the equipment (Inasmet-Tecnalia, Spain) using argon as the only plasma gas. All samples were made under the same thermal spraying conditions (Demnati *et al* 2011). The number of runs was varied from 1 to 20 and a total of 12 runs were selected to build up the thickness of the coating.

2.2. Powders and coatings characterization

Powders were subjected to thermogravimetric analysis (TGA) with a heating rate of 5 °C min^{-1} between 30 and 1400 °C under argon gas (Labsys Setaram TG-DTA, France) to analyze the thermal behavior during heating and phase transformations. The cooling rate was set at 99 °C min^{-1}.

X-ray diffraction analyses on both ClA and HA feedstock powders and scrapped off coatings were carried out using a Seifert XRD-3000 diffractometer (Cu$K_{\alpha 1}$ radiation; step-scan: 24 s; step: 0.02°; 2θ range: 20°–60°). The HA coatings crystallinity ratio was evaluated in accordance with the international standards (ISO 13779–3:2008). It is based on the following equation (ISO 13779–3:2008):

$$Cr = \frac{\sum A_{(hkl)}}{\sum A'_{(hkl)}} * 100, \quad (2)$$

where Cr is the crystallinity ratio of HA coatings, Σ $A_{(hkl)}$ the sum of the integrated area of ten HA coating diffraction peaks and Σ $A'_{(hkl)}$ the sum of the integrated area of ten powder (fully crystallized HA reference powder) diffraction peaks (table 1). The same approach was used to determine the crystallinity ratio of ClA coatings and the ten most intense diffraction lines for ClA phase are reported in table 1.

FTIR spectroscopy analyses of the initial powders and of the scraped coatings were performed by transmission using KBr pellets (4 cm^{-1} resolution) and a FTIR spectrometer (Nicolet 5700, France). For this purpose, each powder or removed coating was dispersed in a KBr matrix (1 mg of sample in 150 mg of KBr).

Table 1. The ten most intense diffraction lines of HA and ClA phases considered for the calculation of the crystallinity ratio of HA and ClA coatings, respectively.

HA diffraction lines	ClA diffraction lines
002	201
102	002
210	210
211	211
112	300
300	112
202	202
310	310
222	222
213	213

2.3. SBF test on coatings

SBF solution was prepared by a method derived from that described in ISO standard 23317 and by Kokubo (Kokubo 1998), involving a separation of precipitable anions and cations. Two solutions (anions and cations) were prepared at physiological pH (7.25) at 37 °C and mixed in equal proportion to give the final SBF solution with mineral ion concentrations close to those of human blood plasma (table 2). The coated samples were immersed in 100 mL of SBF solution placed in vials covered with lids and maintained at 37 °C. After 28 days of immersion in the same solution, the samples were removed from the fluid, rinsed in distilled water then dried at 60 °C overnight according to the ISO standard 23317.

The surface of samples was observed by SEM. The samples were then analyzed by XRD. A few micrograms of the Ca/P layer formed on the surface of HA or ClA coatings after immersion in SBF were scraped off. This was mixed with KBr and pressed into plates for analysis using infrared (FTIR) spectroscopy.

Table 3. Theoretical and experimental chemical composition (wt%) of ClA and HA powders.

Sample	(%) Ca ± 0.5%	(%) P ± 0.5%	(%) Cl ± 0.5%	Ca/P ratio ± 0.02%
ClA (exp)	38.2	17.7	6.0	1.67
ClA (th)	38.5	17.8	6.8	1.67
HA (exp)	38.1	17.8	–	1.67
HA (th)	39.9	18.5	–	1.67

3. Results and discussion

3.1. Powders characterization

The conversion reaction from HA to ClA powder was achieved after 30 min. The fast conversion time prevented particle growth and a change in powder properties. The particle size distribution and morphology of HA and ClA powders were similar. Chemical analyses of both the ClA and HA powders are summarized in table 3. The calcium content of apatite powders was determined by complexometry with ethylenediaminetetraacetic acid and the phosphorus content by spectrophotometry of the phosphovanadomolybdic complex (Charlot 1966).

The Ca/P ratio for both ClA and HA powders corresponds to stoichiometric apatites. The x-ray patterns of ClA and HA powders are shown in figures 2(*a*) and 3(*a*), respectively. They are characteristics of pure, well-crystallized apatite. In the case of ClA, the monoclinic variety (JCPDS 01–70-1454) was obtained, whereas the pattern of HA corresponded to that of the hexagonal structure (JCPDS 09–432); no foreign crystallized phase was detected. At room temperature, the monoclinic structure should be obtained with both compositions; however, commercial HA usually exhibits a hexagonal structure. This anomaly is generally attributed to the presence of impurities, always present in trace amounts. In the case of ClA, such

Table 2. Anionic and cationic solution composition used for the preparation of SBF solution and ion concentrations of SBF and human blood plasma.

Cationic solution (1L)		Anionic solution (1 L)	
Reagents	Weight (g)	Reagents	Weight (g)
NaCl	8.035	NaCl	8.035
KCl	0.450	K_2HPO_4. 3 H_2O	0.462
$MgCl_2$. 6 H_2O	0.622	Na_2SO_4	0.144
$CaCl_2$. 2 H_2O	0.774	TRIS[a]	10
C(HCl) = 1M	39	$NaHCO_3$	0.710

Ion concentrations of SBF and human blood plasma		
Ion	Concentration (10^{-3} mol) in SBF concentration (pH 7.40)	Concentration (10^{-3} mol) in blood plasma (pH 7.2 to 7.4)
Na^+	142.7	142.0
K^+	5.0	5.0
Mg^{2+}	1.5	1.5
Ca^{2+}	2.6	2.5
Cl^-	148.8	103.0
HCO_{3-}	4.2	27.0
HPO_4^{2-}	1.0	1.0
SO_4^{2-}	0.5	0.5

[a] TRIS: trishydroxymethylaminomethane.

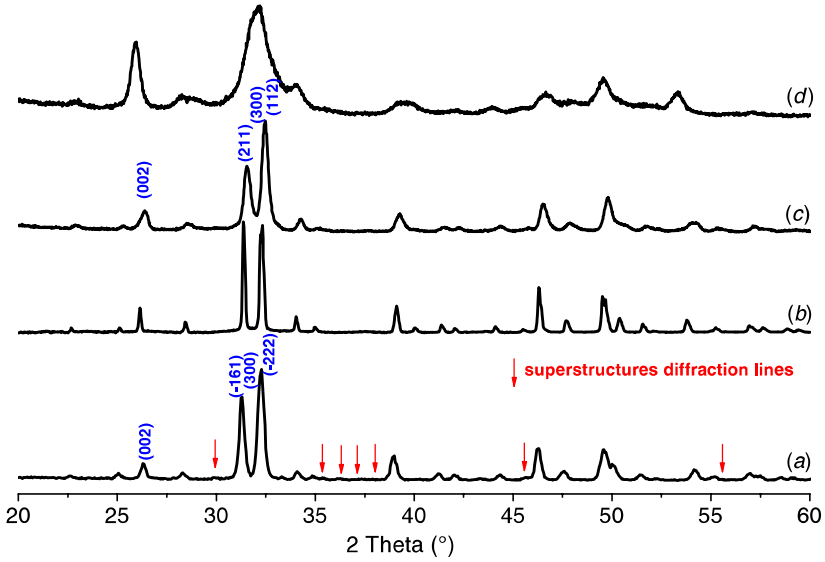

Figure 2. X-ray patterns of ClA powders (*a*), ClA powder after TGA heat treatment (*b*), as sprayed ClA coating (*c*) and ClA coating after four weeks of immersion in SBF (*d*) nanocrystalline apatite analogous to bone mineral.

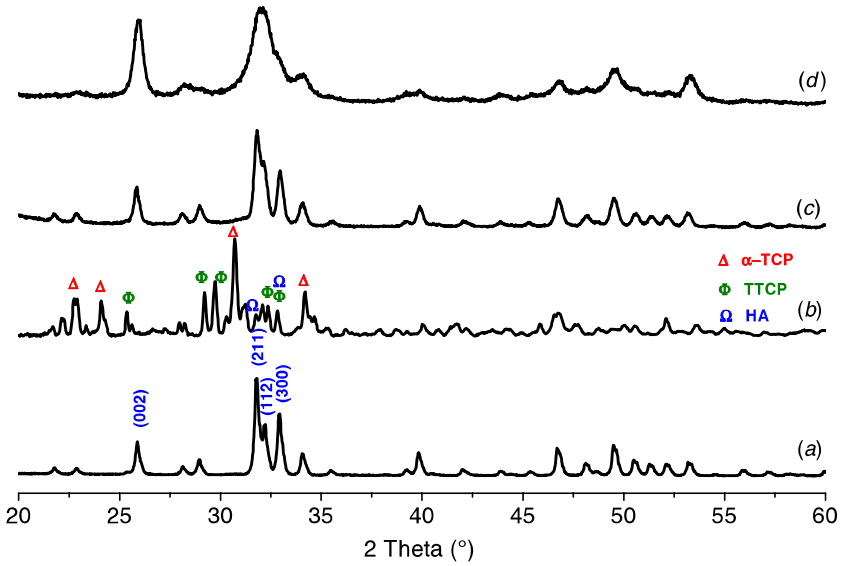

Figure 3. X-ray patterns of HA powders (*a*), HA powder after TGA heat treatment (*b*), as sprayed HA coating (*c*) and HA coating after four weeks of immersion in SBF (*d*) nanocrystalline apatite analogous to bone mineral.

impurities could have been removed as volatile chlorides during the conversion of HA into ClA (Lacout 1983), thus favoring the phase transition at a low temperature (185–210 °C).

The FTIR spectra of both ClA and HA powders are shown in figures 4(*a*) and 5(*a*), respectively. The most intense absorption bands at 460, 550–600, 960 and 1020–1120 cm^{-1} are characteristic of phosphate groups. The additional bands at 630 and 3572 cm^{-1} in the HA powders spectra have been assigned to OH groups. These bands were completely absent from the spectra of ClA powders. The absence of OH groups means that OH^- ions were substituted by chloride ions during the experiment.

3.2. Thermal stability of apatite phases

The TGA curves of the HA and ClA powders are presented in figure 6. During the heating of HA, we can see (i) a weak weight increase close to 0.1% in the range of 40–800 °C: this phenomenon was previously linked to water sorption on the surface by Trombe (Trombe 1972); (ii) an important weight loss beginning at 830 °C was then observed showing slope changes at 1360 °C: this weight loss has been assigned to a water release corresponding to the dehydroxylation of HA (Trombe 1972, Gross *et al* 1998). The first part of the weight loss (800–1360 °C) seems to correspond to the formation of oxy-HA (OHA) according to the following equation:

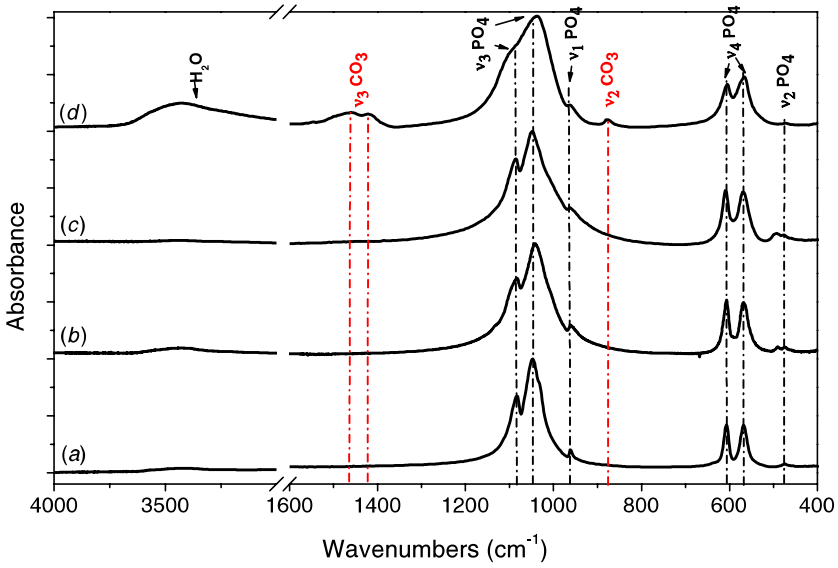

Figure 4. FTIR spectra of ClA powders (*a*), ClA powder after TGA heat treatment (*b*), as sprayed ClA coating (*c*) and ClA coating after four weeks of immersion in SBF (*d*) nanocrystalline apatite analogous to bone mineral.

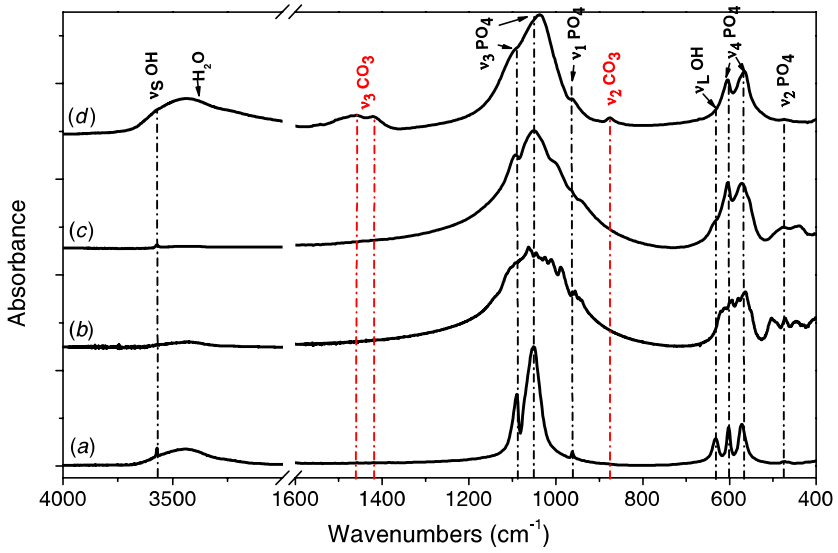

Figure 5. FTIR spectra of HA powders (*a*), HA powder after TGA heat treatment (*b*), as sprayed HA coating (*c*) and HA coating after four weeks of immersion in SBF (*d*) nanocrystalline apatite analogous to bone mineral.

$$Ca_{10}(PO_4)_6(OH)_2 \rightarrow Ca_{10}(PO_4)_6(OH)_{2-2x}O_x\square_x + xH_2O. \quad (3)$$

The second part (starting at 1360 °C) with an accelerated water release can be assigned to the decomposition of OHA (Trombe 1972, Gross *et al* 1998), according to the phase diagram (Gross and Berndt 1998), to give a mixture of TCP and TTCP according to the following reaction:

$$Ca_{10}(PO_4)_6(OH)_{2-2x}O_x\square_x \rightarrow 2Ca_3(PO_4)_2 + Ca_4O(PO_4)_2 + (1-x)H_2O. \quad (4)$$

This acceleration is induced by the formation of new phases which facilitate the decomposition of the remaining OH species at an increased rate as the diffusion of water in the apatite lattice is not a limiting step. The maximal temperature was limited to 1400 °C, but a previous study highlighted that the HA decomposition continues at a higher temperature (Elliott 1994).

During the cooling, two phenomena appear: the first one from 1400 to 650°C corresponding to a weight increase (at 1290 °C) could be linked to a partial reverse reaction (3 and 4) between residual water and high temperature phases (TCP, TTCP and OA). The weight loss at lower temperature (about 400 °C) could be due to the surface desorption of water.

The ClA exhibits poor weight loss in the thermal domain explored compared to HA. However, two weak phenomena at 90 and 200 °C can be seen. The first corresponding to the desorption of surface water, and the second could be attributed to the decomposition of residual NH_4Cl also pointed

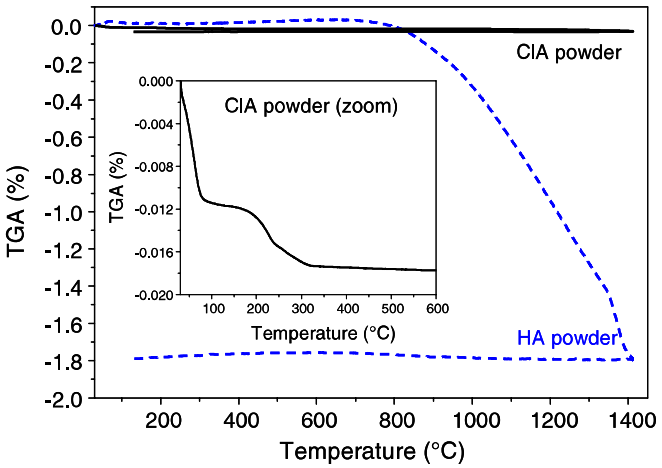

Figure 6. TGA curves of ClA and HA powders.

out in a previous study (Demnati 2011). This constituent has condensed during the cooling stage of the solid–gas synthesis of ClA using NH_4Cl.

Figure 5(*b*) showed the FTIR spectra of the heat-treated HA powder. The stretching band υ_SOH at 3572 cm^{-1} corresponding to the OH groups has disappeared and the libration OH band at 630 cm^{-1} decreased and appeared as a shoulder. The main phosphate bands (υ_3PO_4 and υ_4PO_4) showed less resolution and decomposition than those observed for the initial HA powder spectrum. The υ_2PO_4 phosphate band was relatively intense and appeared much stronger than that in the initial powder. The absence of the υ_SOH band and the increase of the intensity of the υ_2PO_4 band are assigned to oxyapatite (OA) (Ranz 1996, Yang *et al* 1995). However, υ_3PO_4 and υ_4PO_4 bands were characteristics of TCP and TTCP.

The typical x-ray patterns of the HA powder after TGA heating are shown in figure 3(*b*). The peaks of HA are barely observed and the diagram exhibits mainly the peaks of α-TCP and TTCP. These results support the hypothesis of the partial HA decomposition (Gross *et al* 1998, Trombe 1972, Elliott 1994). Reversible reactions (equation (3) and (4)) allow the recovery of the initial HA phase, nevertheless water is required but gas was continually purged.

The FTIR spectrum of the ClA powder after heating (figure 4(*b*)) exhibited the same vibration bands as the initial ClA powder spectrum, but relatively broad bands, especially the υ_3PO_4. The x-ray patterns of ClA after TGA are very close to those of ClA initial powder confirming the good stability of the powder in this temperature range. Nevertheless, we can note that peaks on figure 2(*b*) exhibit a lower full width at half maximum (FWHM) compared to those of the initial powder. This result indicated an increase of the crystallinity induced probably by (i) the sintering of grains and (ii) the decrease of the entropy due to the annealing facilitated at this temperature.

In the literature (Prener 1971, Elliott 1994), these 'opposite' temperature behaviors are attributed to a higher mobility of the hydroxyl group compared to that of chloride in the anion column of the apatitic structure. This decreased ion mobility could also be related to the cell size variations. In the case of ClA, this modification may stabilize (Prener 1971, Elliott 1994) the chloride ions in the restricted volume in the column, and a higher energy is probably required to allow its mobility. Contrary to HA, ClA exhibits a melting point but thermal decomposition before melting could be possible, but were not reported.

In the case of HA, the thermal decomposition (Elliott 1994) in two steps is related to the formation of OHA. In this case, the water loss and hydroxyl replacement by O^{2-} occurred when two hydroxyl groups react in the solid and release a water molecule. However, the mechanism of ClA decomposition is rather different, according to Prener (Prener 1971), ClA, heated under vacuum, loose $CaCl_2$ to give non-stoichiometric apatites:

$$Ca_{10}(PO_4)_6\,Cl_2 \rightarrow x\,CaCl_2 + Ca_{10-x}(PO_4)_6\,Cl_{2(1-x)}. \quad (5)$$

This reaction can eventually lead to decomposition into α-TCP and $CaCl_2$:

$$Ca_{10}(PO_4)_6\,Cl_2 \rightarrow CaCl_2 + 3Ca_3(PO_4)_2. \quad (6)$$

The kinetics of these reactions have not been investigated; it seems however that there is no high temperature loss in our TGA data and that these reactions might not appear for the heating times involved.

Although, the TGA data confirm the thermal stability of ClA compared to HA, the significance of these results on plasma sprayed coatings characteristics can be questioned. Heat and mass transfer phenomena which are of crucial importance are difficult to address and only a few publications report on these generally proposing models (Pawlowski 2008, Dyshlovenko *et al* 2005). Regarding the composition of the HA coatings, most authors refer to the phase diagram which despite their inadequacy for non-equilibrium processes such as plasma spraying (Heimann 2006, Gross and Berndt 1998), allow a prediction of the coating composition.

3.3. Coatings characterization

The x-ray pattern of the as-sprayed ClA coatings can be seen in figure 2(*c*). In terms of phase composition, a single phase of apatite corresponding to JCPDS file 33–271 was detected and no other peaks could be observed. Moreover, x-ray patterns corresponded to the high crystallinity samples. This is in agreement with the crystallinity ratio of ClA-coatings, which was calculated to be around 98%. A transition from the monoclinic to the hexagonal space group $P6_3/m$ has been reported. This transition was mentioned to be held between 185 and 210 °C (Elliott 1994, Prener 1971).

The x-ray diffraction patterns of HA coatings show that all peaks correspond to crystalline HA without any other crystalline phases. However, the presence of a small amount of amorphous phase can be distinguished (small diffuse halo). The calculated crystallinity ratio was equal to 68%.

Figures 4(*c*) and 5(*c*) showed the FTIR spectra of the as-sprayed coatings surface, highlighting spectral characteristics of ClA and HA. Bands at 480, 585–608, 964 and 1085–1042 cm^{-1} correspond to the vibration modes of the PO_4 group (Rey *et al* 1989, Elliott 1994). A thin OH^- absorption band at 3750 cm^{-1} can be seen in HA-coatings spectra.

The surface morphologies of the as-sprayed ClA and HA coatings (12 spray runs) are shown in figures 7(*a*) and 8(*a*), respectively. The observations of the coating surfaces show

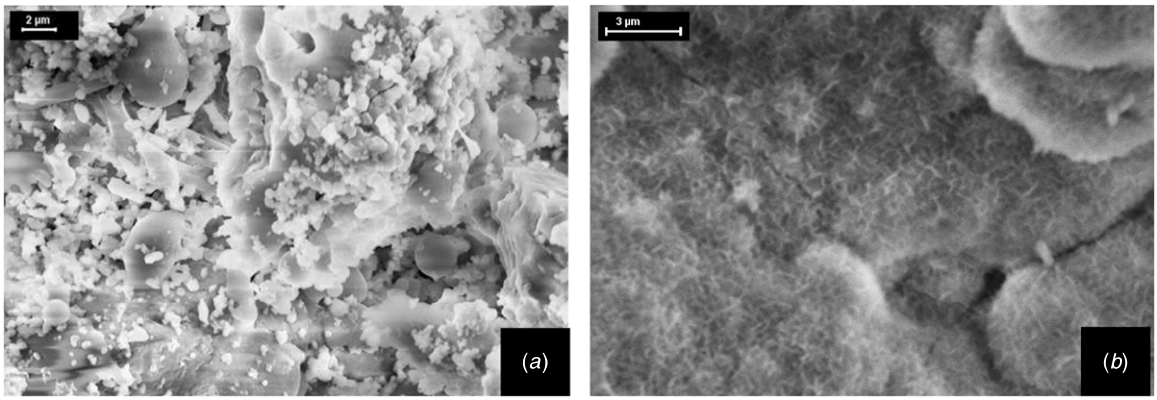

Figure 7. SEM micrographs of 12 run ClA coating surface before (*a*) and after SBF treatment (*b*).

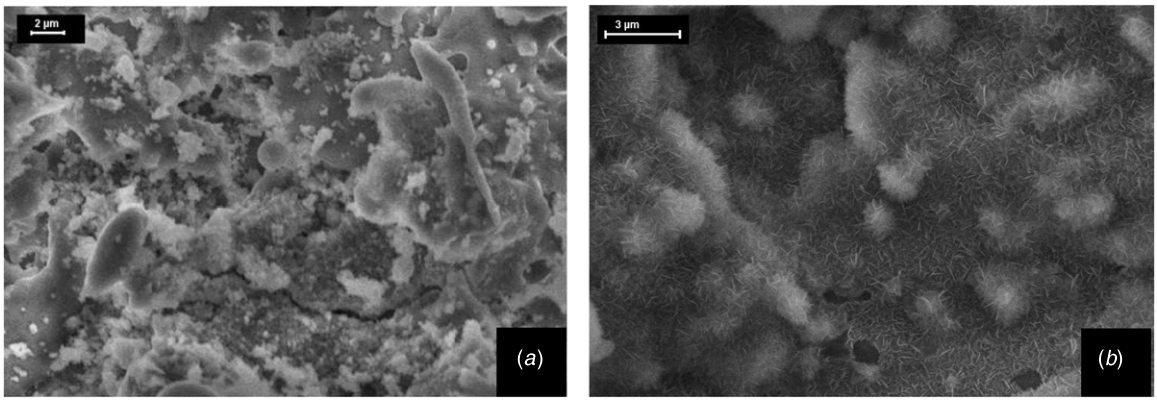

Figure 8. SEM micrographs of 12 run HA coating surface before (*a*) and after SBF treatment (*b*).

a typical lamellar microstructure characteristic of plasma-sprayed coatings. Furthermore, the surface was rough with the presence of small pores and spherical particles of different sizes. However, no cracks were observed. Nevertheless, the comparison of the two coatings (ClA and HA) shows a lower roughness of the ClA-coating surface than of the HA coating. It seems that the texture of ClA coatings is different from that of HA coatings. After a detailed examination of collected micrographs, it can be observed that small recrystallized particles and partially recrystallized splats constitute the dense and rough surface of the ClA coatings. However, HA coatings were mainly composed of flattened particles over small amount of partially melted and unmelted particles. In the literature, several studies can be found on the modeling of the behavior of particles during the impact on the substrate (St Doltsinis *et al* 1998). Due to the very low thermal conductivity of apatites (HA or ClA) and the little time that apatite particles spend in-flight in the plasma flame, a high thermal gradient occurred inside each in-flight particle during plasma spray processing. Moreover, the phase diagram allows us to predict phase composition (Carayon and Lacout 2003) even if plasma spray conditions are very far from thermodynamic equilibrium conditions. In addition, due to the high temperature of the flame, the external part of the grain is essentially composed of a liquid phase. In the case of HA, the liquid phase is probably associated with calcium oxide (CaO). The high melting point (2855 °C) of the CaO and its observation in the coatings imply that the Ca/P ratio has decreased in the liquid phase. The underlying zone of the grain particle would not melt; however, it could probably decompose to give α-TCP, TTCP and CaO. The internal core of the HA particle, will be partially dehydroxylated but the apatitic structure should not be altered. This core should be the nearest to a HA structure and composition. This phenomenon has been previously described by Heimann (Heimann 2006).

After impact on the substrate, these particles take different complex forms. The fast quenching also allows important temperature gradients in the coating formed. The lamellar calcium phosphate splats formed are extremely heterogeneous and the different domains are overlapped at the microcrystalline scale (Li *et al* 2004). Different reactions are involved in this case (Heimann 2006). Even if the thermodynamical conditions of the plasma spray process are far from the equilibrium conditions of the phase diagram, most of the studies on HA plasma spraying highlighted the presence of phases mentioned in the phase diagram (Deram *et al* 2003, Gross and Berndt 1998, Heimann 2006, Cheang and Khor 1996).

The absence of CaO, TCP and TTCP and the low proportion of the amorphous phase (ACP) from the resulting HA coatings made by the LEPS system are rather surprising. In fact, the presence of ACP phases considered to be formed from the rapid quenching of a liquid phase attest that temperature in the in-flight particles was above 1600 °C. However, the phases resulting from the decomposition of the OHA in the 1300–1600 °C domains were not detected by x-ray diffraction.

Gross and Berndt reported that a fast cooling rate after quenching could inhibit the formation of those phases (Gross and Berndt 1998). The cooling rate is difficult to measure; however, we suppose that it is higher with the LEPS system than with the conventional plasma spray system. This difference is attributed to the small particle range (50–80 μm), to the short stand-off-distance (40 mm) and the low energy of the new system (15 kW) (Demnati *et al* 2011). Furthermore, a re-formation of the OHA from the molten phase was suspected and this re-formation induces the establishment of diffusion during the fast cooling of the molten phase.

The study of the ClA coating surface by x-ray diffraction and FTIR spectroscopy shows a mineralogically pure phase without any crystalline impurity. A fine examination of the FTIR spectra shows bands (especially an intense ν_2PO_4 band and a splitted ν_1PO_4) which have been considered to be characteristics of OA and which are also found in the HA coating. The formation of OA or oxy-chlorapatite (Ox-ClA) must be considered. However, no OH groups were observed in the as-sprayed ClA coatings. To our knowledge, no work in the literature has mentioned the formation of an Ox-ClA phase. The hypothesis of the presence of a solid solution of an Ox-ClA was strengthened after previous studies (Demnati 2011). Similar observations were reported for fluor-hydroxyapatite coatings (Ranz 1996). Assuming that the ClA used was completely chlorinated as it did not contain detectable OH groups able to induce OA formation, it seems likely that there is a parasite reaction during spraying. Two hypotheses may exist: (i) chloride–oxygen exchange involving atmospheric oxygen or (ii) ClA hydroxylation with water vapor in the gas or the powder. Reactions that are susceptible to form an Ox-ClA during plasma spraying are the following:

$$Ca_{10}(PO_4)_6(Cl)_2 + x/2O_2 \rightarrow Ca_{10}(PO_4)_6(Cl)_{2-2x}O_x\square_x + xCl_2 \quad (7)$$

$$Ca_{10}(PO_4)_6(Cl)_2 + 2xH_2O \rightarrow Ca_{10}(PO_4)_6(Cl)_{2-2x}O_x\square_x + xH_2O + 2xHCl. \quad (8)$$

Different points remain unclear and questionable including the assumption that we issued at the beginning of this discussion, which suggests the presence of an apatitic core inside each particle (Heimann 2006, Gross *et al* 1998). Other investigators argued that the grains melt completely during the plasma spraying of the liquid and recrystallized in calcium phosphate phases (Sun *et al* 2001, De Groot *et al* 1987).

Indeed, based on the phase diagram, the decomposition of apatites is completely reversible on cooling. In this case, the nature of the phases present after cooling and the crystallinity of the coating depend mainly on the cooling conditions and on the substrate temperature which in turn determine the development of recombination reactions, nucleation and crystal growth.

3.4. SBF testing

The SBF solution is a supersaturated aqueous medium that simulates the inorganic ions composition in body fluid. The SBF could allow us to predict the material bioactivity. According to Kokubo and Takama (2006).

Table 4. Crystallite size of apatite phase after soaking in SBF for 28 days.

	L_{002} ($\pm$ 5 Å)	L_{310} ($\pm$ 5 Å)	L_{002}/L_{310}
ClA coating	164	66	2.48
HA coating	159	65	2.45
Human bone[a]	213	68	3.13

[a] Medium value for a long bone (Ranz 1996).

After 28 days of soaking in the SBF solution, a significant difference in the surface morphology of the coatings can be clearly observed (figures 7(*b*) and 8(*b*).). The SEM observations for both ClA and HA surface implants (figures 7(*b*) and 8(*b*)) showed the formation of a thin film composed by ball-like grains and numerous cracks which differ completely from the original morphology of the as-sprayed coating. At a higher magnification, very small crystallites of nanocrystalline apatite can be observed.

X-ray patterns of ClA coatings and HA coatings after the SBF test are presented in figures 2(*d*) and 3(*d*), respectively. XRD patterns of the samples showed reflections characteristic of a poorly crystalline apatite. No other crystalline phase was observed. The broad and overlapping reflections attest the low crystallinity of apatite formed. The crystallite sizes of the 12-run ClA and HA coatings were calculated by the Scherrer equation from the XRD profiles of the (0 0 2) and (3 1 0) reflections and the values are summarized in table 4. A preliminary examination of the values shows that the crystals formed during the test have nanometric dimensions close to those of bone mineral crystals especially closer to young bone crystals (smaller size).

The FTIR spectra of the ClA and HA coatings soaked in the SBF solution for 28 days are also given in figures 4(*d*) and 5(*d*). In addition to phosphate bands, bands at 886 and 1420–1467 cm^{-1} are due, respectively, to the ν_2 and ν_3 carbonate groups absorption. A weak water absorption band around 3400 cm^{-1} can also be seen.

The FTIR spectrum of the coatings immersed in SBF showed the formation of carbonated apatite (CA) on the surface of the coatings. The occurrence of this phase could result from two phenomena: (i) the nucleation and growth on the coating, by epitaxy, of apatite nanocrystals from the supersaturated SBF solution or/and (ii) a hydrolysis reaction involving the crystallization and conversion of the amorphous phase at the surface of the coating into apatite. It has been demonstrated that non-apatitic labile environments correspond to surface species on the nanocrystals can be detected by the decomposition of phosphate and carbonate domains of FTIR spectra (Rey *et al* 1996).

We focused on the ν_4PO_4 and ν_2CO_3 domains to investigate the evolution of non-apatitic hydrogenophosphate and carbonate ions. Figure 9 shows the decomposition of the ν_4PO_4 band spectra for both ClA and HA coatings. These decompositions were made considering Lorentzian bands for each peak. In the ν_4PO_4 domain, we note the presence of rather weak bands corresponding to HPO_4^{2-} and PO_4^{3-} non-apatitic groups situated at 535 and 617 cm^{-1}. The decomposition in the ν_2CO_3 domain (figure 10) show, in addition to specific

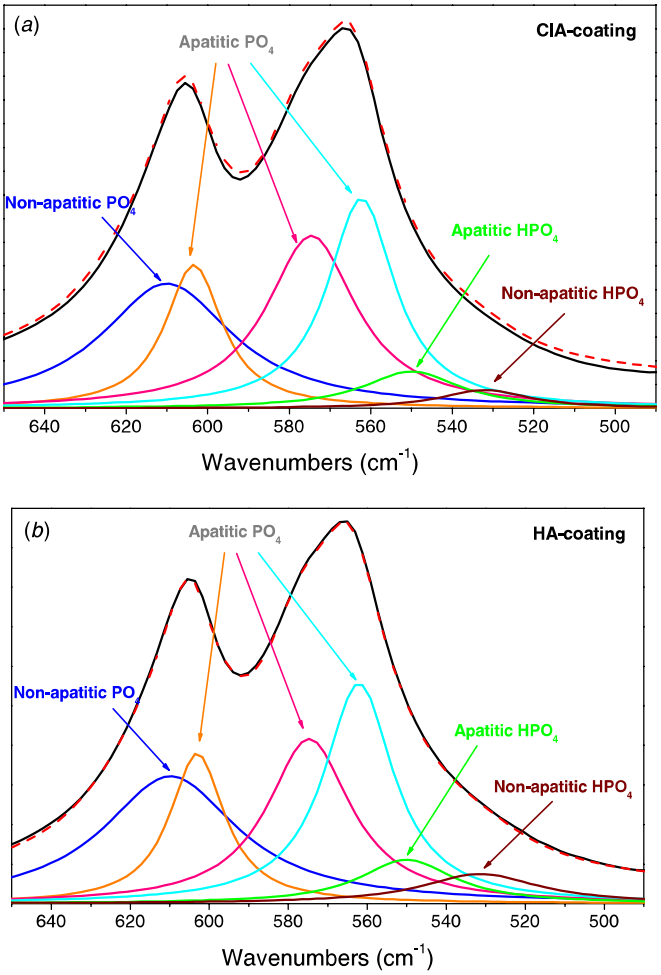

Figure 9. ν_4PO_4 FTIR band decomposition for (*a*) ClA and (*b*) HA coatings.

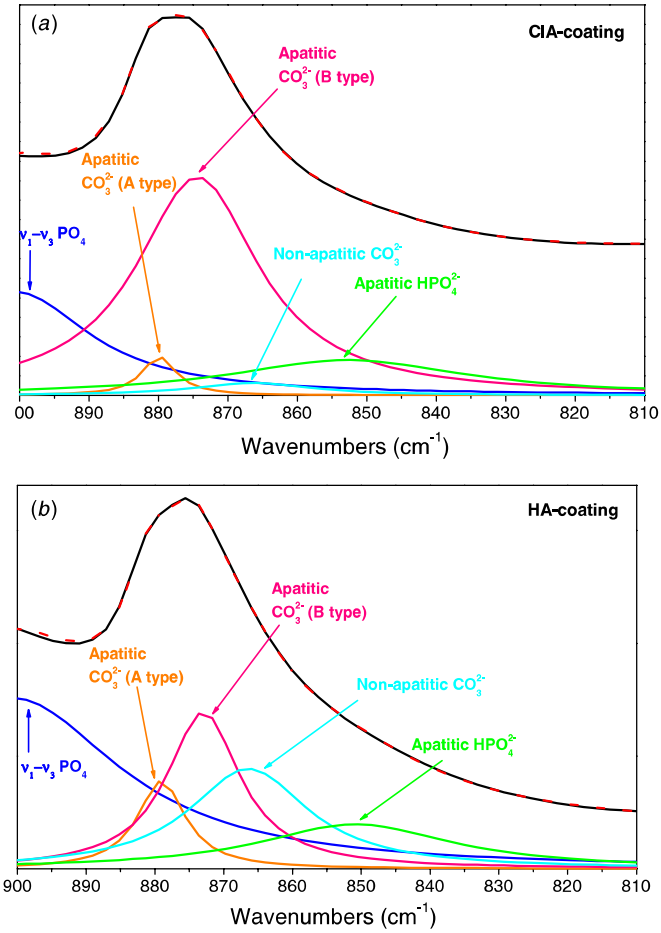

Figure 10. ν_2CO_3 FTIR band decomposition for (*a*) ClA and (*b*) HA coatings.

bands of type A and B carbonate ions, a broad band at 866 cm^{-1} characteristic of labile carbonate present at the surface of apatite nanocrystals (Rey 1998).

The *in vitro* test realized in this work allows one to obtain a layer composed of carbonated apatite nanocrystals of low crystallinity on the coating surface, whatever the coating initial composition (HA or ClA) be. This phenomenon attests the reactivity of apatite coatings studied and suggests, according to Kokubo, that we could expect a good osteoconductivity from the coatings developed by the LEPS system. This *in vitro* test is a first step in assessing the possible bioactivity of ClA and *in vitro* cell culture and *in vivo* implantations have been performed to further evaluate if there is an advantage of using ClA coatings.

4. Conclusion

In this paper, ClA and HA powders have been elaborated to perform thin coatings by a novel LEPS device. The ClA was synthesized by solid–gas reaction between commercial HA and ammonium chloride. The easy and fast synthesis allows us to obtain a pure and stoichiometric ClA powder. In addition, the evaluation of the behavior of apatite powders at high temperature by TGA analysis confirmed the thermal stability of ClA.

Otherwise, microstructure shows well-crystallized coatings without decomposed phases (TCPs, TTCP or CaO) which are classically detected in conventional plasma sprayed HA coatings. In summary, these results indicate that the plasma spraying parameters were well optimized and the ClA has a better thermal behavior than HA: the crystallinity ratio was higher and the amorphous phase and the oxyapatite amounts were lower than in HA. In addition, ClA and HA coatings made by the LEPS device were able to form a thin film of carbonated apatite analogous to bone mineral in SBF solution. However, in a biological environment, which is an open system, the calcium phosphate behavior may be different. It must be noted that interactions between the material and living environment are numerous and complex.

Acknowledgments

This study was carried out under a MNT ERA-Net Project named NANOMED2. The authors gratefully thank the Midi-Pyrénées region for financial support for research carried out in the CIRIMAT Laboratory (France), and the Basque government and Tratamientos Superficiales Iontech,

SA for their financial and technical support under the IG-2007/0000381 grant for the development of the LEPS device and deposition of the coatings carried out in INASMET-Tecnalia. Industrial French collaborators (TEKNIMED SA and 2PS SA) were financed by OSEO programs.

References

Carayon M and Lacout J 2003 Study of the Ca/P atomic ratio of the amorphous phase in plasma-sprayed hydroxyapatite coatings *J. Solid State Chem.* **172** 339–50

Charlot G 1966 Les méthodes de la chimie analytique, Masson

Cheang P and Khor K 1996 Addressing processing problems associated with plasma spraying of hydroxyapatite coatings* 1 *Biomaterials* **17** 537–44

Cheng K, Weng W, Wang H and Zhang S 2005 *In vitro* behavior of osteoblast-like cells on fluoridated hydroxyapatite coatings *Biomaterials* **26** 6288–95

De Groot K, Geesink R, Klein C and Serekian P 1987 Plasma sprayed coatings of hydroxylapatite *J. Biomed. Mater. Res.* **21** 1375–81

Demnati I 2011 Développement et caractérisation de revêtements bioactifs d'apatite obtenus par projection plasma à basse énergie: application aux implants biomédicaux *Thèse de Doctorat* de l'Institut national polytechnique de toulouse

Demnati I, Parco M, Grossin D, Fagoaga I, Drouet C, Barykin G, Combes C, Braceras I, Goncalves S and Rey C 2011 Hydroxyapatite coating on titanium by a low energy plasma spraying mini-gun *Surf. Coat. Technol.* **206** 2346–53

Deram V, Minichiello C, Vannier R N, Le Maguer A, Pawlowski L and Murano D 2003 Microstructural characterizations of plasma sprayed hydroxyapatite coatings *Surf. Coat. Technol.* **166** 153–9

Dyshlovenko S, Pawlowski L, Pateyron B, Smurov I and Harding J H 2005 Modelling of plasma particle interactions and coating growth for plasma spraying of hydroxyapatite *Surf. Coat. Technol.* **200** 3757–69

Elliott J C 1994 *Structure and Chemistry of the Apatites and other Calcium Orthophosphates* (Amsterdam: Elsevier)

Gross K A and Berndt C C 1998 Thermal processing of hydroxyapatite for coating production *J. Biomed. Mater. Res.* **39** 580–7

Gross K A, Berndt C C, Stephens P and Dinnebier R 1998 Oxyapatite in hydroxyapatite coatings *J. Mater. Sci.* **33** 3985–91

Heimann R B 2006 Thermal spraying of biomaterials *Surf. Coat. Technol.* **201** 2012–9

Kokubo T 1998 Apatite formation on surfaces of ceramics, metals and polymers in body environment *Acta Mater.* **46** 2519–27

Kokubo T and Takadama H 2006 How useful is SBF in predicting *in vivo* bone bioactivity? *Biomaterials* **27** 2907–15

Lacout J L 1983 Contribution à l'étude de l'extraction par vapométallurgie du manganèse et du vanadium des apatites *Thèse de Doctorat* de l'Institut national polytechnique de toulouse

Li H, Khor K and Cheang P 2004 Thermal sprayed hydroxyapatite splats: nanostructures, pore formation mechanisms and TEM characterization *Biomaterials* **25** 3463–71

Pawlowski L 2008 *The Science and Engineering of Thermal Spray Coatings* (New York: Wiley)

Prener J 1971 Nonstoichiometry in calcium chlorapatite *J. Solid State Chem.* **3** 49–55

Ranz X 1996 Développement et caractérisation de dépôts d'apatite obtenus par projection plasma sur prothèses orthopédiques *Thèse de Doctorat de l'Institut national polytechnique de toulouse*

Rey C 1998 Calcium phosphates for medical applications *Calcium Phosphates in Biological and Industrial Systems* ed Z Amjad (Dordrecht: Kluwer)

Rey C, Collins B, Goehl T, Dickson I and Glimcher M 1989 The carbonate environment in bone mineral: a resolution-enhanced Fourier transform infrared spectroscopy study *Calcif. Tissue Int.* **45** 157–64

Rey C, Hina A, Somrani S, Jemal M and Glimcher M J 1996 Chemical properties of poorly crystalline apatites *Phosphorus Res. Bull.* **6** 67–70

St Doltsinis I, Harding J and Marchese M 1998 Modelling the production and performance analysis of plasma-sprayed ceramic thermal barrier coatings *Arch. Comput. Methods Eng.* 59–59

Sun L, Berndt C C, Gross K A and Kucuk A 2001 Material fundamentals and clinical performance of plasma sprayed hydroxyapatite coatings: a review *J. Biomed. Mater. Res.* **58** 570–92

Tõnsuaadu K, Gross K A, Plūduma L and Veiderma M 2011 A review on the thermal stability of calcium apatites *J. Therm. Anal. Calorim.* 1–13

Trombe J C 1972 Contribution a l'étude de la décomposition et de la réactivité de certaines apatites hydroxylées, carbonatées ou fluorées alcalino-terreuses *Thèse de Doctorat* de l'Université Paul-Sabatier Toulouse, Sc. phys. Toulouse III. 1972. No 501

Yang C, Wang B, Chang E and Wu J 1995 The influences of plasma spraying parameters on the characteristics of hydroxyapatite coatings: a quantitative study *J. Mater. Sci.: Mater. Med.* **6** 249–57

Young R and Elliott J 1966 Atomic-scale bases for several properties of apatites *Arch. Oral Biol.* **11** 699–707